

PAPER

Symbolic time series analysis of fNIRS signals in brain development assessment

To cite this article: Zhenhu Liang *et al* 2018 *J. Neural Eng.* **15** 066013

View the [article online](#) for updates and enhancements.



IOP | ebooks™

Bringing you innovative digital publishing with leading voices to create your essential collection of books in STEM research.

Start exploring the collection - download the first chapter of every title for free.

Symbolic time series analysis of fNIRS signals in brain development assessment

Zhenhu Liang^{1,2} , Yasuyo Minagawa³, Ho-ching Yang², Hao Tian¹,
Lei Cheng¹, Takeshi Arimitsu⁴, Takao Takahashi⁴ and Yunjie Tong^{2,5}

¹ Institute of Electrical Engineering, Yanshan University, Qinhuangdao 066004, People's Republic of China

² Weldon School of Biomedical Engineering, Purdue University, West Lafayette, IN, United States of America

³ Faculty of Letters, Department of Psychology, Keio University, Tokyo, Japan

⁴ Department of Pediatrics, Keio University School of Medicine, Tokyo, Japan

E-mail: tong61@purdue.edu (Y Tong)

Received 1 June 2018, revised 10 September 2018

Accepted for publication 12 September 2018


Published 28 September 2018



Abstract

Objective. Assessing an infant's brain development remains a challenge for neuroscientists and pediatricians despite great technological advances. As a non-invasive neuroimaging tool, functional near-infrared spectroscopy (fNIRS) has great advantages in monitoring an infant's brain activity. To explore the dynamic features of hemodynamic changes in infants, in-pattern exponent (IPE), anti-pattern exponent (APE), as well as permutation cross-mutual information (PCMI) based on symbolic dynamics are proposed to measure the phase differences and coupling strength in oxyhemoglobin (HbO) and deoxyhemoglobin (Hb) signals from fNIRS. **Approach.** First, simulated sinusoidal oscillation signals and four coupled nonlinear systems were employed for performance assessments. Hilbert transform based measurements of hemoglobin phase oxygenation and deoxygenation (hPod) and phase-locking index of hPod (*hPodL*) were calculated for comparison. Then, the IPE, APE and PCMI indices from resting state fNIRS data of preterm, term infants and adults were calculated to estimate the phase difference and coupling of HbO and Hb. All indices' performance was assessed by the degree of monotonicity (DoM). The box plots and coefficients of variation (CV) were employed to assess the measurements and robustness in the results. **Main results.** In the simulation analysis, IPE and APE can distinguish the phase difference of two sinusoidal oscillation signals. Both *hPodL* and PCMI can track the strength of two coupled nonlinear systems. Compared to *hPodL*, the PCMI had higher DoM indices in measuring the coupling of two nonlinear systems. In the fNIRS data analysis, similar to hPod, the IPE and APE can distinguish preterm, term infants, and adults in 0.01–0.05 Hz, 0.05–0.1 Hz, and 0.01–0.1 Hz frequency bands, respectively. PCMI more effectively distinguished the term and preterm infants than *hPodL* in the 0.05–0.1 Hz frequency band. As symbolic time series measures, the IPE and APE were able to detect the brain developmental changes in subjects of different ages. PCMI can assess the resting-state HbO and Hb coupling changes across different developmental ages, which may reflect the metabolic and neurovascular development. **Significance.** The symbolic-based methodologies are promising measures for fNIRS in estimating the brain development, especially in assessing newborns' brain developmental status.

Keywords: brain development, symbolic dynamic, fNIRS, in-pattern exponent and anti-pattern exponent, permutation cross mutual information

 Supplementary material for this article is available [online](#)

(Some figures may appear in colour only in the online journal)

⁵ Author to whom any correspondence should be addressed.

1. Introduction

Evaluating brain development is always a challenge in neuroscience and a clinical concern for the pediatricians. Existing studies indicate that earlier exposure to the extra-uterine environment (Watanabe *et al* 2017), postmenstrual age (Arimitsu *et al* 2018), birth weight (Streimish *et al* 2012), and the intrauterine/neonatal insults (Mwaniki *et al* 2012, Thomason *et al* 2017) may influence preterm infants' brain developmental trajectories. Preterm infants have a higher rate of neurodevelopmental diseases than term infants (Volpe 2009, Watanabe *et al* 2017). However, present studies still lack effective methods to access neonates' brain development status.

Functional near-infrared spectroscopy (fNIRS) is an optical brain imaging tool used in neuroscience. With the portable and non-invasive characteristics, as well as the merit of being tolerated by infants and children, the fNIRS is more suitable for assessing neonates' brain development (Quaresima *et al* 2012, Issard and Gervain 2018). fNIRS also allows bedside monitoring for long periods. All these features give unique advantages of fNIRS over functional Magnetic Resonance Imaging (fMRI) in the studies of newborns (Benavides-Varela *et al* 2017, Issard and Gervain 2017).

In developmental neuroscience, fNIRS studies of infants have shown that the hemodynamic response has canonical and non-canonical responses and changes with age in different cognitive tasks and brain regions (Lloyd-Fox *et al* 2017, Issard and Gervain 2018). In term and preterm infants, Watanabe *et al* found that the time-averaged phase differences between oxyhemoglobin (HbO) and deoxyhemoglobin (Hb) in spontaneous low-frequency oscillation (<0.1 Hz) were highly correlated with the chronological age (CA) (Watanabe *et al* 2017). The phase of oxygenation and deoxygenation hemoglobin (hPod) changes from in-phase to anti-phase as the CA increases. More fluctuations in hPod values were found in early preterm infants than in late preterm and term infants before 40 weeks postmenstrual age. However, early preterm infants had a slower development at later CAs (i.e. after eight–13 weeks). Furthermore, Taga *et al* employed the hPod and the phase-locking index of hPod ($hPod_L$) to investigate the spatial variation in infants' developing brain cortex (Taga *et al* 2018). They found that hPod exhibited spatial dependency in different brain development stages. Significant $hPod_L$ increases occurred in three-month-old infants compared to the neonate group. All these studies suggest that the dynamic phase difference between HbO and Hb have potential value in assessing the development of underlying neurovascular functions, as well as hemodynamic and metabolic changes, in infants.

In these studies, the instantaneous phase estimated in hPod and $hPod_L$ methodologies are based on the Hilbert transform, which is based on the assumption that the signal has narrow frequency band and stationary (Cohen *et al* 1999, Oliveira and Barroso 1999). However, brain development is a complex process that may be influenced by nonlinear circulatory and neurovascular developmental changes in different states, especially in infants (Norman and O'Kusky 1986, Franceschini *et al* 2007, Roche-Labarbe *et al* 2010). Many studies have

shown that brain activities' dynamic responses measured by fNIRS signals are very likely to be nonlinear (Khoa *et al* 2008, Pouliot *et al* 2012). Nonlinearity from neural activity, blood flow, and metabolism makes the evaluations based on linear analyzing methods inadequate (Bießmann *et al* 2011, Fantini 2014, Sassaroli *et al* 2016). Moreover, oscillations are a prevalent feature of neuronal and hemodynamic recordings. Some methods used to analyze these physiological oscillations assume that they are largely sinusoidal (Cole and Voytek 2017). However, physiological oscillations are usually pseudo-periodic and contain multiple physiological fluctuations (Cole and Voytek 2017). Phase synchronization measurement is an important methodology used to interpret the mechanisms of electrophysiological and hemodynamic variations in cognitive neuroscience and mental diseases. Unfortunately, most phase synchronization analytical methods based on the Fourier transform and Hilbert transform cannot optimally represent a non-stationary signal (Li *et al* 2011).

The biological system's nonlinear characteristics have motivated researchers to investigate its underlying mechanism via nonlinear methodologies. Various measurements have been proposed for fNIRS signal analysis, such as wavelet phase coherence (Tan *et al* 2016), graph theory (Homae *et al* 2010), entropy (Gu *et al* 2017, Perpetuini *et al* 2018), and mutual information (Dalmis and Akin 2015, Yin *et al* 2015). In all these nonlinear measures, the symbolic dynamic analysis is an important nonlinear measurement, which has been widely applied to physiological system analysis (Edwards *et al* 2001, Daw *et al* 2003, Ray 2004, Bießmann *et al* 2011). A central procedure of the symbolic dynamic analysis is discretizing unprocessed time-series records into a corresponding sequence of symbols by comparing neighboring time-series (Bandt and Pompe 2002). Amigo *et al* stated that the signal's ordinal patterns are not only ad hoc symbols but also contain quantitative information regarding the underlying data's temporal scale (Amigo *et al* 2015). Due to the advantages described above, various symbolic dynamic-based measurements, such as permutation entropy, symbolic transfer entropy, and permutation min-entropy, have been widely used in neurological disease diagnosis and brain state monitoring (Martini *et al* 2011, Ferlazzo *et al* 2014, Zunino *et al* 2015), especially in fNIRS recording analysis (Gu *et al* 2017). A multi-scale symbolic information-theory approach has also been proposed to discriminate delayed synchronization and anticipated synchronization (Montani *et al* 2015). In this study, we propose two new exponents based on the patterns of symbolic dynamics, namely in-pattern exponent (IPE) and anti-pattern exponent (APE), to measure the phase relationship between HbO and Hb.

Although many synchronization measurements have been proposed, detecting the weak couplings in physiological recordings remains challenging considering the complex, nonlinear, and nonstationary characteristics of a physiological system (Palus and Vejmelka 2007, Bahraminasab *et al* 2008). Symbolic dynamic-based permutation analysis and conditional mutual information were proposed to estimate the weak coupling in two cardiorespiratory series (Bahraminasab

et al 2008). The similar approaches have been used to estimate neuronal population coupling during seizures (Li and Ouyang 2010) and EEG oscillations in patients under anesthesia (Liang et al 2015). It was suggested that the permutation cross mutual information (PCMI) approach can track time-dependent coupling strength changes, which is associated with a better anti-noise effect. This encouraged us to utilize the PCMI in measuring HbO and Hb coupling in fNIRS and apply it to distinguishing brain development at different stages.

In this study, we used the IPE and APE, as well as PCMI, which are derived from symbolic dynamics and information theory to assess the brain development changes at different stages. These methods were applied to the same data as the hPod and $hPod_L$ methods proposed in the previous literature (Watanabe et al 2017, Taga et al 2018). The whole process is described below: section 2 presents IPE, APE, PCMI, hPod, $hPod_L$ and statistical analysis methods used in detail. In section 3, comparisons are made based on simulated sinusoidal oscillations, coupled nonlinear models are described in detail. An analysis of fNIRS recordings in preterm and term infants and adults based on these measures is detailed in section 4. Finally, the discussion and conclusions are presented in section 5.

2. Methods

2.1. IPE and APE

Symbolic dynamic measurements used to encode nonlinear systems based on time-series analysis have been systematically described in previous studies (Daw et al 2003, Ray 2004). In this study, we explored the temporal interrelationship of specific patterns in two time-series (i.e. HbO and Hb signals). The resulting exponent was used to evaluate the degree of in-phase or anti-phase in these two time-series. The percentage of in-phase and anti-phase measurements was calculated as an exponent to measure synchronization in these two time-series. We termed these two indices IPE and APE, to separate from the phase measures of the Hilbert transform. An algorithm of the diagram was shown in figure 1. When the embedding dimension $m = 3$, there are $3! = 6$ patterns (as shown in figure 1(A)). We termed these 6 patterns as $M \# 1$ to $M \# 6$. For these 6 patterns, the anti-pattern pairs and in-pattern pairs were shown in figure 1(B). The calculation of IPE and APE is straightforward. For two time series, such as HbO and Hb, the symbolic patterns can be constructed at each time point using a moving window. Then, the number of in-pattern pairs N_i and anti-pattern pairs N_a can be achieved. If the data length is L , the maximum number of in-pattern pair or anti-pattern pairs would be $L - m + 1$. Finally, the IPE and APE can be calculated as shown below:

$$\begin{cases} \text{IPE} = \frac{N_i}{L-m+1} \times 100\% \\ \text{APE} = \frac{N_a}{L-m+1} \times 100\%. \end{cases} \quad (1)$$

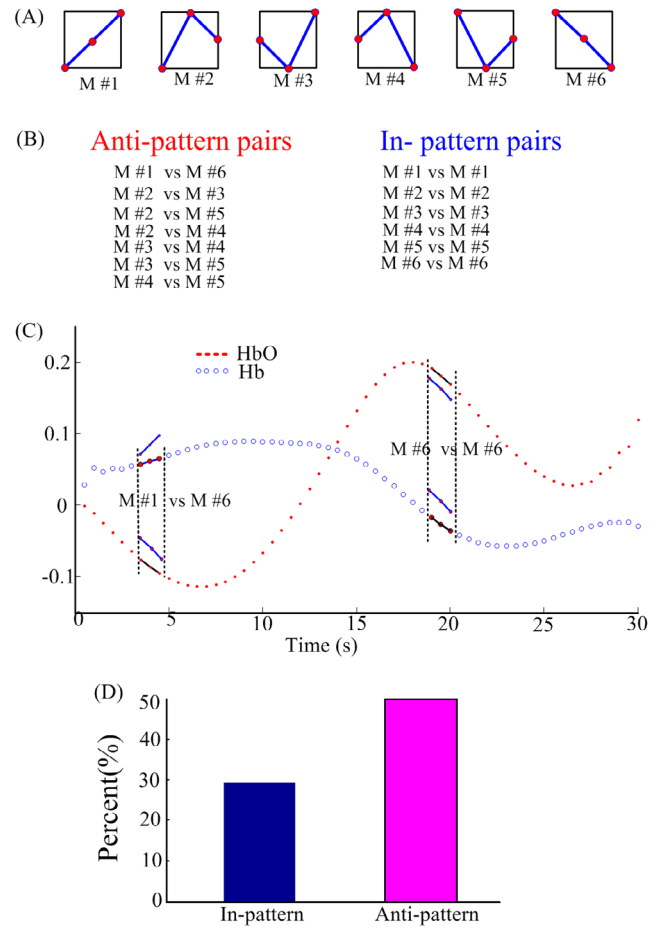


Figure 1. The diagram of anti-pattern and in-pattern percent measurements. (A) The motifs of the order 3 (3!). (B) The lists of the anti-pattern and in-pattern pairs. (C) Two original hemodynamic parameters (HbO and Hb) epochs of 30s segments. In the time point near 5s, the patterns of HbO and Hb are anti-pattern with each other ($M \# 1$ versus $M \# 6$). While the patterns of HbO and Hb are in-pattern with each other at the time near 20s ($M \# 6$ versus $M \# 6$). (D) The in-pattern and anti-pattern percent of the signal in (C).

When $m \geq 4$ the symbolic patterns can describe more sophisticated signals, however, the in-pattern pairs and anti-pattern pairs will become much more complicated than when $m = 3$. Since the hemodynamic changes are relatively slow, the choice of $m = 3$ is sufficient. A more detailed description of the parameter selection was shown in supplementary appendix B (stacks.iop.org/JNE/15/066013/mmedia).

2.2. Permutation cross mutual information (PCMI)

Mutual information is a measurement of synchronization based on information theory, which calculates the amount of shared information between two time-series (Paluš 1996). The PCMI proposed by Li et al (Li and Ouyang 2010) has been applied to estimate the synchronization between two EEG signals (Liang et al 2015, 2016b). The details of PCMI are described as follows:

- (i) A phase space reconstruction method was used to construct the vectors $X_t[x_t, x_{t+\tau}, \dots, x_{t+m\tau}]$ and

$Y_t[y_t, y_{t+\tau}, \dots, y_{t+m\tau}]$ based on two time series of $x(t)$ and $y(t)$, $t = 1, 2, \dots, n$ where m and τ are the embedding dimension and time lag, respectively.

- (ii) X_t and Y_t were ranked in increasing order, $[x_{t+(j_1-1)\tau} \leq x_{t+(j_2-1)\tau} \leq \dots \leq x_{t+(j_m-1)\tau}]$ and $[y_{t+(j_1-1)\tau} \leq y_{t+(j_2-1)\tau} \leq \dots \leq y_{t+(j_m-1)\tau}]$, respectively.
- (iii) Probability distribution functions of the time series $x(t)$ and $y(t)$ were calculate based on the emerged probability of ordinal patterns and termed $p(x)$ and $p(y)$.

The entropy of X_t and Y_t is defined as follows:

$$H(X) = - \sum_{j=1}^J p_j(x) \log p_j(x) \quad (2)$$

and

$$H(Y) = - \sum_{j=1}^J p_j(y) \log p_j(y) \quad (3)$$

- (iv) The joint probability function of X_t and Y_t is termed as $p(x, y)$. The joint entropy of $H(X, Y)$ is defined as

$$H(X, Y) = - \sum_{x \in X} \sum_{y \in Y} p(x, y) \log p(x, y). \quad (4)$$

- (v) The PCMI of time series X_t and Y_t is described as

$$\text{PCMI}(X; Y) = H(X) + H(Y) - H(X, Y). \quad (5)$$

The embedding dimension m is crucial in PCMI calculation, same as the lag τ that is the number of sample points spanned by each section of the motif (Li and Ouyang 2010). A detailed description of the parameters' selections is shown in supplementary appendix C.

2.3. hPod and hPod_L

hPod and hPod_L are the two measurements of phase synchronization. The hPod algorithms described in Watanabe et al (2017) are similar to the spatial analytic phase difference index presented in Pockett et al (2009). And the hPod_L measurement is a classical phase-locking value proposed by Lachaux et al (1999) and has been widely used in the neurophysiological signal analysis (Li et al 2011, Wang et al 2014). Considering two time-series of $x(t)$ and $y(t)$, the calculations of hPod and hPod_L are described as below.

- (1) The analytic signal representation of $x(t)$ and $y(t)$ was calculate based on the Hilbert transform.

$$\begin{cases} x_a(t) = x(t) + jHT[x(t)] \\ y_a(t) = y(t) + jHT[y(t)] \end{cases} \quad (6)$$

Where the $HT[\cdot]$ is the Hilbert transform.

- (2) The signal's instantaneous phase (IP) was estimated:

$$\varphi_x(t) = \tan^{-1} \frac{\text{Im}(x_a(t))}{\text{Re}(x_a(t))} \quad \text{and} \quad \varphi_y(t) = \tan^{-1} \frac{\text{Im}(y_a(t))}{\text{Re}(y_a(t))}.$$

- (3) hPod was calculated based on the IP. Because the IP is wrapped around $[-\pi, \pi]$, we needed to unwrap the IP on the real axis. Firstly, we estimated the absolute difference between the IP of φ_x and φ_y , termed $\Delta\varphi_{xy}$. Then, $\Delta\varphi_{xy}$ was projected into the interval $[0, 2\pi]$. Finally, to achieve a consistent phase range with the measure in Watanabe et al (2017), the phase differences in the $[0, \pi]$ range were projected into the $[\pi, 2\pi]$ range.

- (4) hPod_L was calculated. The measurement of hPod_L is defined as:

$$hPod_L = \frac{1}{N} \left| \sum_{t=1}^N e^{j\Delta\phi_{xy}(t)} \right|. \quad (7)$$

Where the N is the length of the time series $x(t)$ and $y(t)$. The hPod_L is bounded between 0 and 1.

2.4. Statistical analysis

The aim of this study was to (1) evaluate the performance of symbolic measurements (i.e. IPE, APE, and PCMI) in assessing the brain developmental stages, and (2) compare them with calculated hPod and hPod_L. Given the indices of hPod are angle values (i.e. different from numerical values), a circular statistics toolbox was used to perform statistical analysis (Berens 2009). The Watson–Williams test was used to evaluate whether the mean phase of two or more groups is identical, and the parametric Watson–Williams multi-sample test was used to determine the significant differences between groups. For other indices, the Lilliefors test (*lillietest.m*) was performed to determine whether the data had a normal distribution. Kruskal–Wallis test (*kruskalwallis.m*) and multiple comparison tests (*multcomare.m*) were used to determine the significant differences between the indices in different age groups. The Bonferroni correction was used to prevent multiple comparison problems with $p < 0.05/(\text{number of channels})$. The coefficient of variation (CV), calculated from the ratio of the standard deviation (SD) over the mean, was employed to assess the index stability in brain development measurements (Li et al 2008).

3. Stimulation and results

3.1. The simulated signals

To evaluate IPE's and APE's performance in phase difference estimation, we simulated two time-series by combining two sinusoid waves with different frequencies across three situations (i.e. in-phase, anti-phase, and orthogonal-phase). Furthermore, two random time-series were used to assess the index's performance in evaluating the noise signals' impact. All the formulas are described as follows:

(1) In phase sinusoid equations

$$\begin{cases} x(t) = 20 \sin(0.4\pi t) + 15 \sin(0.2\pi t) \\ y(t) = 0.3x(t). \end{cases} \quad (8)$$

(2) Anti-phase sinusoid equations

$$\begin{cases} x(t) = 20 \sin(0.4\pi t) + 15 \sin(0.2\pi t) \\ y(t) = 20 \sin(0.4\pi t - \pi) + 15 \sin(0.2\pi t - \pi). \end{cases} \quad (9)$$

(3) Orthogonal-phase sinusoid equations

$$\begin{cases} x(t) = 20 \sin(0.4\pi t) + 15 \sin(0.2\pi t) \\ y(t) = 20 \sin(0.4\pi t + 0.5\pi) + 15 \sin(0.2\pi t + 0.5\pi). \end{cases} \quad (10)$$

Random signals were generated by the MATLAB function *randn.m*. The amplitude of the signal $y(t)$ is three times larger than $x(t)$. The data length of all the simulation signals is 500 s.

3.2. The coupling models

In this study, we employed four models to evaluate the coupling performance of PCMI and $hPod_L$. The coupling strength of bivariate dynamics was controlled by one continuous parameter. The first is the Rossler–Lorenz model (Andrzejak et al 2003):

$$\begin{cases} \dot{x}_1 = -6(x_2 + x_3) \\ \dot{x}_2 = 6(x_1 + 0.2x_2) \\ \dot{x}_3 = 6[(x_1 - 5.7)x_3 + 0.2] \\ \dot{y}_1 = 10(-y_1 + y_2) \\ \dot{y}_2 = 28y_1 - y_2 - y_1y_3 + \varepsilon x_2^2 \\ \dot{y}_3 = y_1y_2 - \frac{8}{3}y_3. \end{cases} \quad (11)$$

The coupling strength parameter ranged from $\varepsilon = 0$ to $\varepsilon = 5$ in a step of 0.2. The discrete time series X_n and Y_n from x_1 and y_1 were resampled at the sampling rate at 40 Hz (Liang et al 2015).

The second model system consisted of two coupled Henon maps proposed in the literature (Schiff et al 1996). The third and fourth models were made by two coupled Rossler (Palus and Stefanovska 2003) and Lorenz systems (Kreuz et al 2007), respectively. In this study, the coupling strength parameter in Henon was ranged from 0 to 0.8 with a step of 0.01. The coupling strength parameters in Rossler and Lorenz systems were set from 0 to 2 in step of 0.025 (Liang et al 2016a).

3.3. Evaluation of the model

We hypothesized that an increased coupling strength is linearly correlated with increased of synchronization. The degree of monotonicity (DoM) was used to evaluate the dependence of $hPod_L$ and PCMI measures on the coupling strength ε (Kreuz et al 2007).

The formula of DoM is as follows:

$$\text{DoM} = \frac{2}{r(r-1)} \sum_{i=1}^{r-1} \sum_{j=i+1}^r \text{sign}(s_j - s_i). \quad (12)$$

Where s_i and s_j are the coupling measure indices (i.e. $hPod_L$ and PCMI) at monotonously-increased coupling strengths. $i, j = 1, 2, \dots, r$ where the parameter r is the number of the discretized coupling strengths. If indices of s monotonically increased with the enhancing coupling strength ε , then $s_i < s_j$, $i \leq j$. DoM = 1 when the sequence of s_1, s_2, \dots, s_r is strictly monotonous increases with the enhanced coupling strengths, while DoM = -1 when the indices monotonically decrease with the increasing coupling strengths.

3.4. Results

To compare IPE's and APE's performance with $hPod$ via the phase relationship between two time-series, we employed simulated and random noise signals. $hPod_L$ and PCMI were also compared in estimating coupling strength in different coupled models. We studied the anti-phases, in-phases, and orthogonal-phases of two sinusoidal signals, which were shown in figures 2(A), S1(A) and S2(A), respectively. Two random noise signals, which had random phase and no coupling between them, were used for assessment (see figure S3(A)). The $hPod$ index was able to accurately reflect anti-phases, in-phases, and orthogonal-phases (see figures 2(B), S1(B) and S2(B)). Like $hPod$, the IPE and APE can precisely measure the same phase difference between these three situations. The IPEs were equal to 1 and 0 in in-phase and anti-phase patterns, respectively (see figures 2(D) and S1(D)). For the orthogonal phase relationship, IPE and APE were distributed around 0.42, which means the percent of anti-patterns and in-patterns in this situation is close to 0.5 (see figure S2(D)). All these results illustrate that the IPE and APE have similar performance in measuring phase differences.

For the coupling strength measurement, the $hPod_L$ indices remained 1 at in-phase, anti-phase, and orthogonal-phase scenarios (see figures 2(C), S1(C) and S2(C)). The analysis of parameter selection presented in supplementary appendix C shows that PCMI with an embedding dimension of $m = 3$, combined with lag $\tau = 11$ is the optimal selection. The PCMI indices in in-phase, anti-phase, and orthogonal-phase patterns were about 1.68, 1.68, and 0.64, respectively. Unlike $hPod_L$, the PCMI measurement regards the orthogonal-phase pattern to be a different coupling pattern from the in-phase and anti-phase patterns. We calculated the cross-correlation index of these two orthogonal-phase signals and we found that the correlation coefficient was equal to 0 when the lag = 0 s. The different results for PCMI, $hPod_L$, and cross-correlation may be derived from the different calculation principles and mechanisms while estimating synchronization (Liang et al 2016b).

Furthermore, the random noise simulation showed that the $hPod$ indices were randomly distributed around the circle (see in figure S3(B)). The $hPod_L$ indices calculated from this time course are ranged from 0 to 0.2, which means that the two

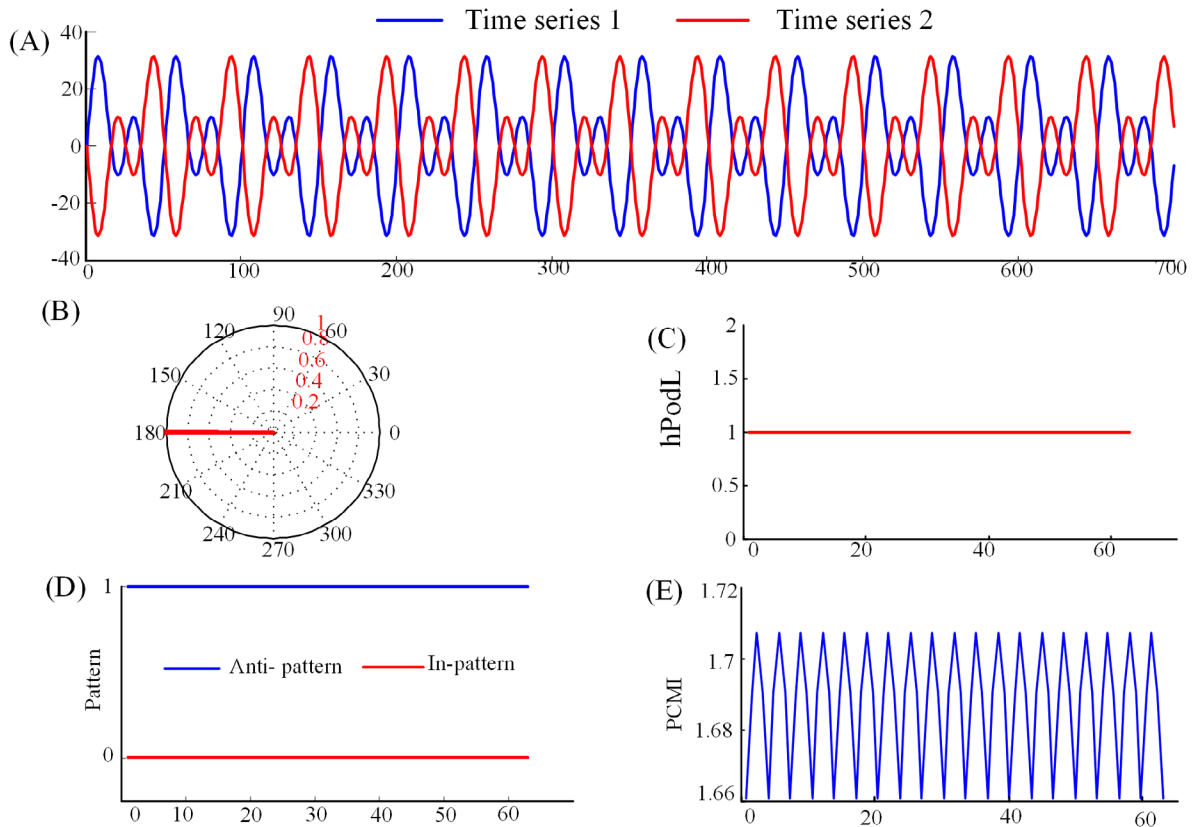


Figure 2. The comparison of the hPod and symbolic dynamic based measurements. (A) Two in-phase time series. (B) The hPod indices of the two time series in (A). (C) The hPod length of the time series in (A). (D) The anti-pattern percent and in-pattern percent values of the two time series. (E) The PCMI indices of the two time series.

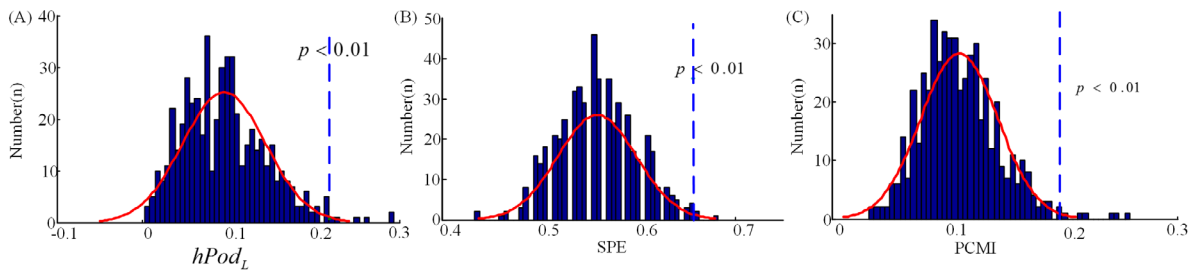


Figure 3. The histogram distributions of $hPod_L$ (A), SPE (B) and PCMI (C) derived from the 500 random time series epochs.

time-series are not correlated with each other. Hence, in this situation, the hPod values are invalid. The IPE and APE of these two random noise signals ranged in 0.1–0.3 and 0.3–0.5, respectively. The PCMI indices ranged from 0.02 to 0.1.

Additionally, to analyze the indices' range in all these measures at random time series, we calculated 500 pairs random noise segments. The distributions of $hPod_L$, as well as the sums of IPE, APE (SPE), and PCMI were presented in figures 3(A)–(C), respectively. Based on these distributions, we proposed a significant threshold for each measure ($p < 0.01$) to avoid spurious results. The significant thresholds of $hPod_L$, SPE and PCMI are 0.20, 0.64 and 0.19, respectively.

$hPod_L$'s and PCMI's performance in tracking the coupling strength was assessed further in four coupled non-linear systems. Figures 4(A) and (B) showed the two simulated datasets in a coupled Rossler–Lorenz system, where coupling strength varied from 0 to 5 with a step

of 0.2. The time series at the coupling strength of $\varepsilon = 0$ and 5 were presented in figures 4(C) and (D). Figure 4(E) showed the $hPod_L$, and PCMI of a coupled Rossler–Lorenz system at different coupling strengths. All three indices showed a rising trend with an increase in coupling strength. However, we also observed an abrupt increase in the coupling strength value around 2.2 that gradually decreased when the coupling strength value was greater than 3.5 in the $hPod_L$ curve (figure 4(E)).

DoM was used to evaluate $hPod_L$'s and PCMI's dependence on the coupling strength. DoM values of $hPod_L$ and PCMI for the coupled Hénon, Rössler, Lorenz, and Rossler–Lorenz (R–L) systems were shown in figure 5. All the DoM values were shown in table 1. Notably, the DoM values of PCMI were higher than those of $hPod_L$ in every model. The results illustrate that the PCMI more accurately assessed coupling strength than $hPod_L$.

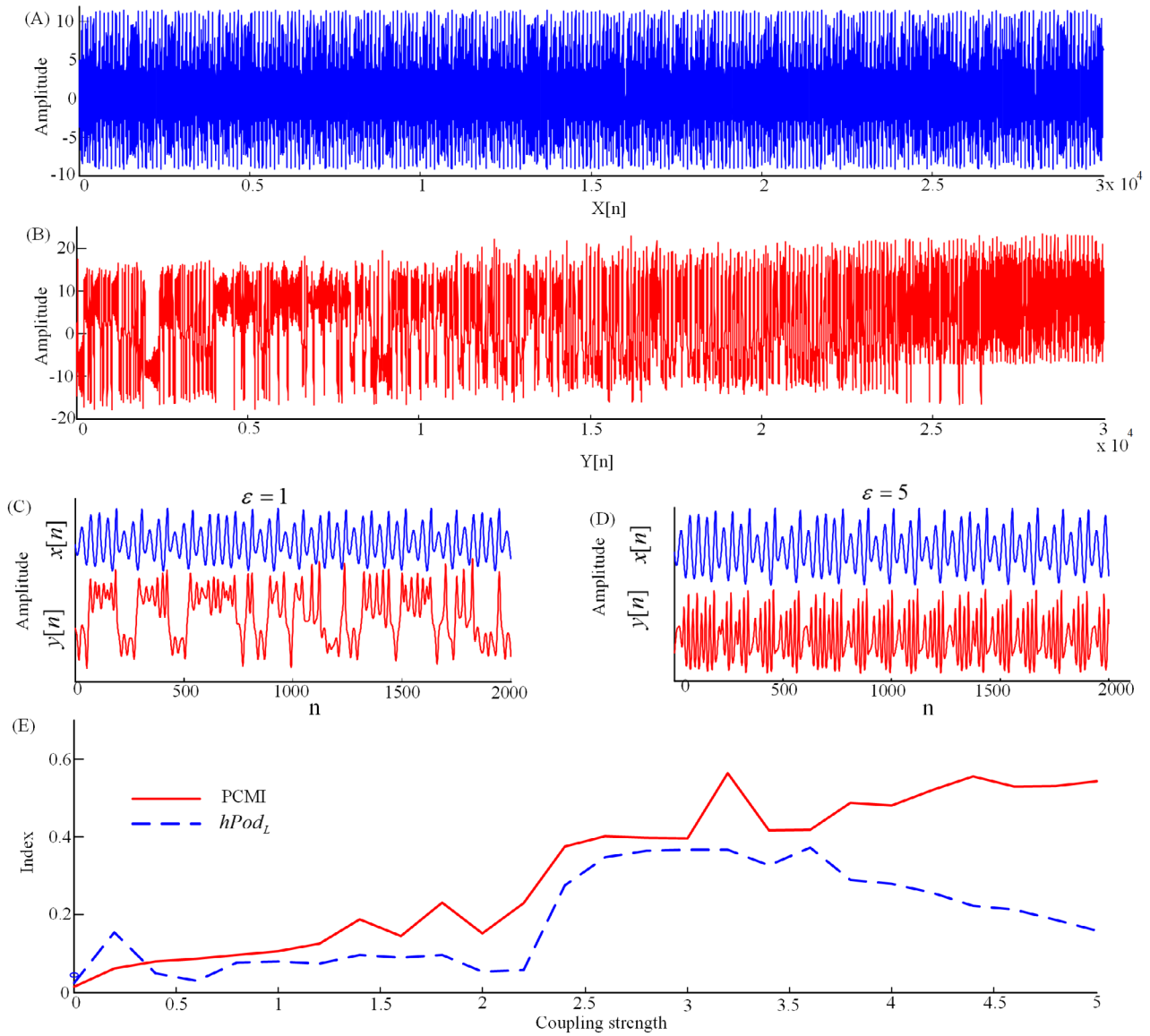


Figure 4. The simulation data generated based on the coupled Rossler–Lorenz model. (A) and (B) are the time series from the variables of v_1 and w_1 in Rossler–Lorenz model with $dt = 0.025$. (C)–(D) Time series of X_n and Y_n at two specific coupling strength $\varepsilon = 0$ and 5. (E) The $hPod_L$ and PCMI indices versus different coupling strength of Rossler–Lorenz system.

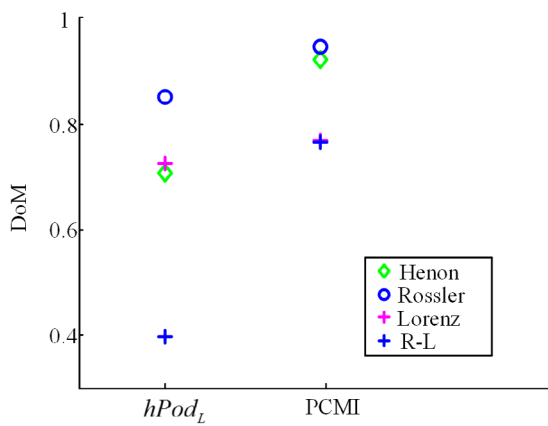


Figure 5. The DoM of $hPod_L$ and PCMI indices for the coupled Henon, Rossler, Lorenz and Rossler–Lorenz systems.

Table 1. The DoM values of $hPod_L$ and PCMI in measuring the model of coupled Henon, Rossler, Lorenz and R–L.

	$hPod_L$	PCMI
Henon	0.70	0.96
Rossler	0.85	0.94
Lorenz	0.73	0.77
R–L	0.40	0.77

4. Applications in fNIRS

4.1. fNIRS data recordings

We analyzed data from ten term infants (six boys and four girls), and ten preterm infants (five boys and five girls) during sleep. A detailed description of the participants was presented

Table 2. Demographic characteristics of the neonates.

Characteristics	Preterm	Term
Total (boy/girl)	10(6/4)	10(5/5)
GA (mean(min-max)) (wk)	32.5 (30.1–33.4)	38.3 (37–39.9)
PNA (day)	23.7 (17–35)	4.2 (3–6)
Birth weight (mean(min-max)) (g)	1644.3(1302–1887)	2874.8 (2476–3936)

GA = Gestational age.

PNA = Post natal age.

wk = week.

in table 2. Ethical approval was obtained from the ethical committee of Keio University Hospital (No. 20090189), and written informed consent was acquired from the participants' parent(s) prior to beginning the test. All the neonates were tested in a dimly-lit room when they were in active sleeping status as judged by their frequent motor activity and rapid eye movements.

A NIRS system (ETG-4000, Hitachi Medical Corporation) with 46 channels was used to measure the relative fluctuations of HbO and Hb concentrations (millimolar millimeter (mM * mm)). Two sets of 3 * 3 array probes were mounted on the left and right temporal regions. And one 3 * 5 holder was mounted on the frontal region. The distance between the source and detector was about 2 cm. The sampling rate of the fNIRS recording was 10 Hz and the wavelengths of NIR lights were 695 and 830 nm. fNIRS coverage included frontal and temporal areas.

To compare developing and mature brains, we enrolled eight adult volunteers (aged 22–40 years, seven male, one female) for resting state testing. A fNIRS neuroimaging system (NIRx, NIRx Medical Technologies, LLC) was used for the experiment. All the volunteers were asked to close their eyes and lay flat on the bed in a dimly-lit room. Volunteers signed the written informed consent approved by the Purdue University ethics committee. The duration of the resting-state NIRS measurement was 15 min and a total of 20 channels were used to cover the prefrontal brain area.

4.2. Data preprocessing

Motion artifact is a major source of noises in fNIRS, especially in clinical tests. In this study, we used a kurtosis-based wavelet filtering for motion artifact correction (Chiarelli *et al* 2015). Figure 6 showed the denoising process of HbO and Hb from one channel. Figure 6(A) presented the HbO and Hb time series before and after denoising. In one example, the transient noise caused by motion was detected at around 250 s. Figure 6(B) showed an example of motion correction for HbO and Hb (between 210 s–270 s). To analyze hemodynamic changes in preterm and term infants and adults, we used a zero-phase digital filter (Matlab function of *filtfilt.m*, the order of butterworth = 3) for band-pass filtering. All the data were motion corrected and resampled to 2 Hz for the further calculation (Pinti *et al* 2015).

In a previous study (Watanabe *et al* 2017), the authors analyzed the hPod of three frequency bands: 0.05–0.1 Hz (main frequency), 0.01–0.05 Hz (low frequency), and 0.1–5 Hz (high frequency, which is dominated by pulsation/respiration and not the focus of our study). To be consistent with the previous study, we analyzed the phase difference and coupling of HbO and Hb in the 0.01–0.05 Hz, 0.05–0.1 Hz, 0.01–0.1 Hz frequency bands. Considering the low cut-off frequency of 0.01 Hz, the data length of IPE, APE, PCMI, hPod, and $hPod_L$ used in the calculation was set as 120 s in 0.01–0.05 Hz and 0.01–0.1 Hz frequency bands. However, in the frequency band of 0.05–0.1 Hz, we have found that the minimum length of the data (i.e. experiment) can be as short as 30 s, which is preferable in the studies of infants. Detailed evaluations can be found in supplementary appendix C and D (we only showed PCMI, which is the most complicated parameter).

4.3. Results

Figure 7 showed the distributions of APE versus IPE for preterm and term infants and adults in the 0.01–0.05 Hz (A), 0.05–0.1 Hz (B) and 0.01–0.1 Hz (C) frequency bands. We averaged the indices for all the channels and each circle represented the scatter distribution of one subject. The distributions of the adults' data were clearly separated from the other two groups (i.e. term and preterm infants) in all three frequency bands. Because IPE and APE are complementary measures, the sum of the in-phase pattern and anti-phase proportions is close to 1 under the slow oscillations of HbO and Hb. For this reason, the IPE and APE indices were mostly scattered around the backslash line, which is a feature of the method we used and does not reflect physiological information. The clear separation of the clustering of IPE and APE along the line indicates the power of the method rather than the line itself. Figure 8 presented the hpod and $hPod_L$ of preterm and term infants and adult subjects in the 0.01–0.05 Hz, 0.05–0.1 Hz, and 0.01–0.1 Hz frequency bands. It was shown that hPod indices of adults are near phase π in all these frequency bands, while the indices of the term and preterm infants are close to $3\pi/2$, especially in the 0.05–0.1 Hz frequency band. The results are similar to those in Watanabe *et al* (2017) and Taga *et al* (2018).

To further investigate the ability of different measures to assess brain development, especially in the term and preterm infants, the indices of each measurement in each channel were considered samples for statistical analysis. A corresponding box plot was presented in figures 9 and 10 for each measurement in each frequency band. In this study, the number of fNIRS recording channels in neonates (preterm and term) and adults are 46 and 20, respectively. To identify significant differences between them, we set the p -value at $p < 0.05/46 = 0.001$. The indices were not normally distributed, so the statistics of the different groups were expressed as medians (min-max), as shown in tables 3–5. The box plots in figure 9 showed that the hPod, IPE and APE of the term and preterm infants and adults differed significantly ($p < 0.0002$). Notably, hPod, IPE, and APE more precisely demarcated

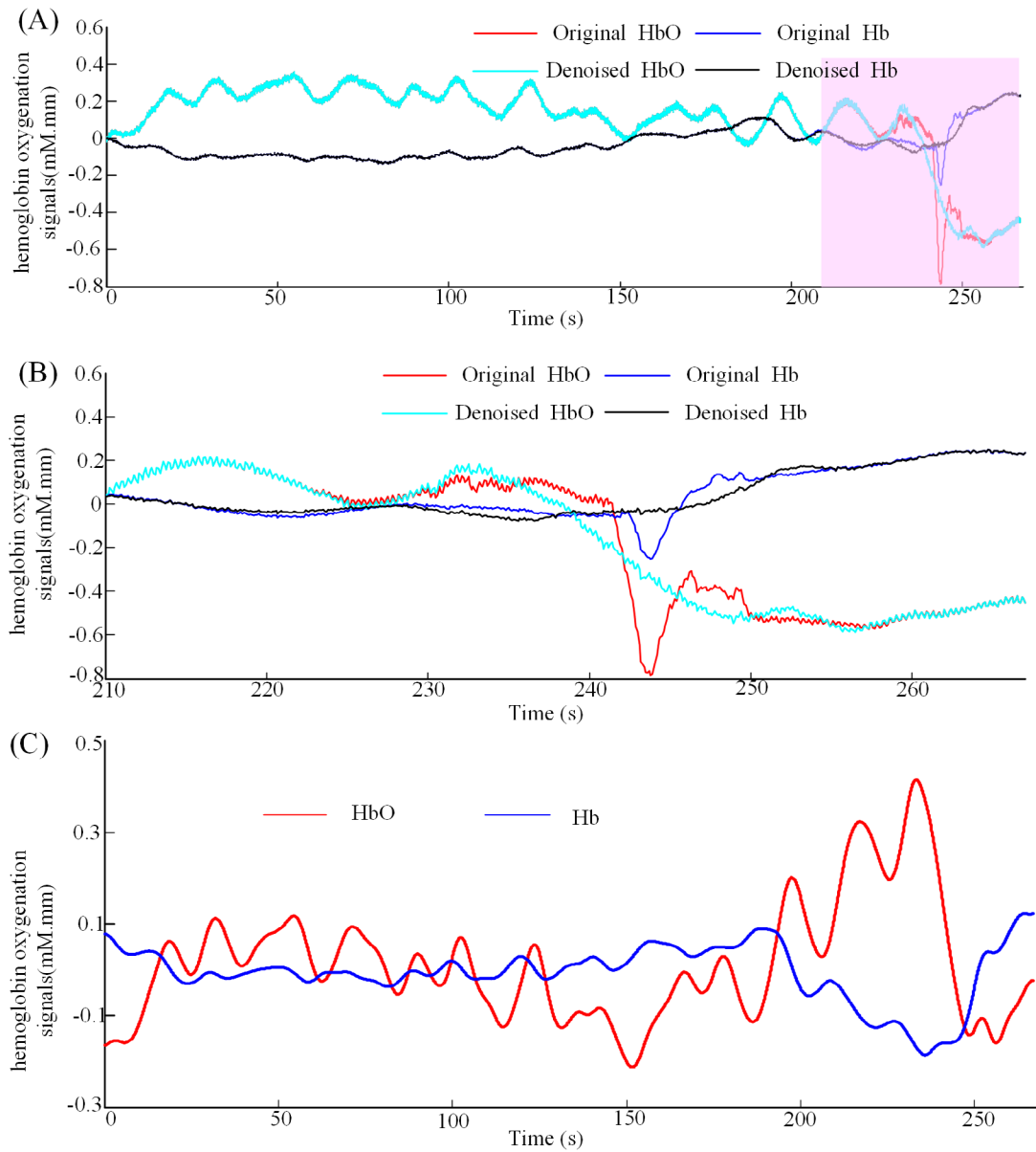


Figure 6. The motion denoising and bandpass filtering of HbO and Hb for one channel. (A) The motion artifact detection and denoising based on the Kurtosis-based wavelet algorithm. The red and blue curves are the original HbO and Hb, respectively. The cyan and black curves are the signals after removal of motion noise. The signals in the time range from 210s to 270s (pink rectangle) were contaminated by head movement. (B) The enlarged signals from the time range from 210s to 270s. (C) The low frequency band signals (0.01–0.1 Hz) of HbO (red) and Hb (blue), respectively.

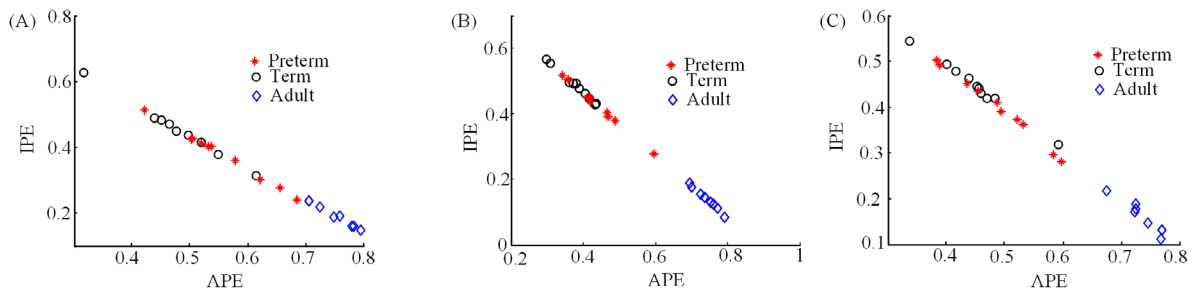


Figure 7. The scatter plot of in-pattern percent versus anti-pattern percent of preterm, term, and adult in 0.01–0.05 Hz (A), 0.05–0.1 Hz (B) and 0.01–0.1 Hz (C), respectively.

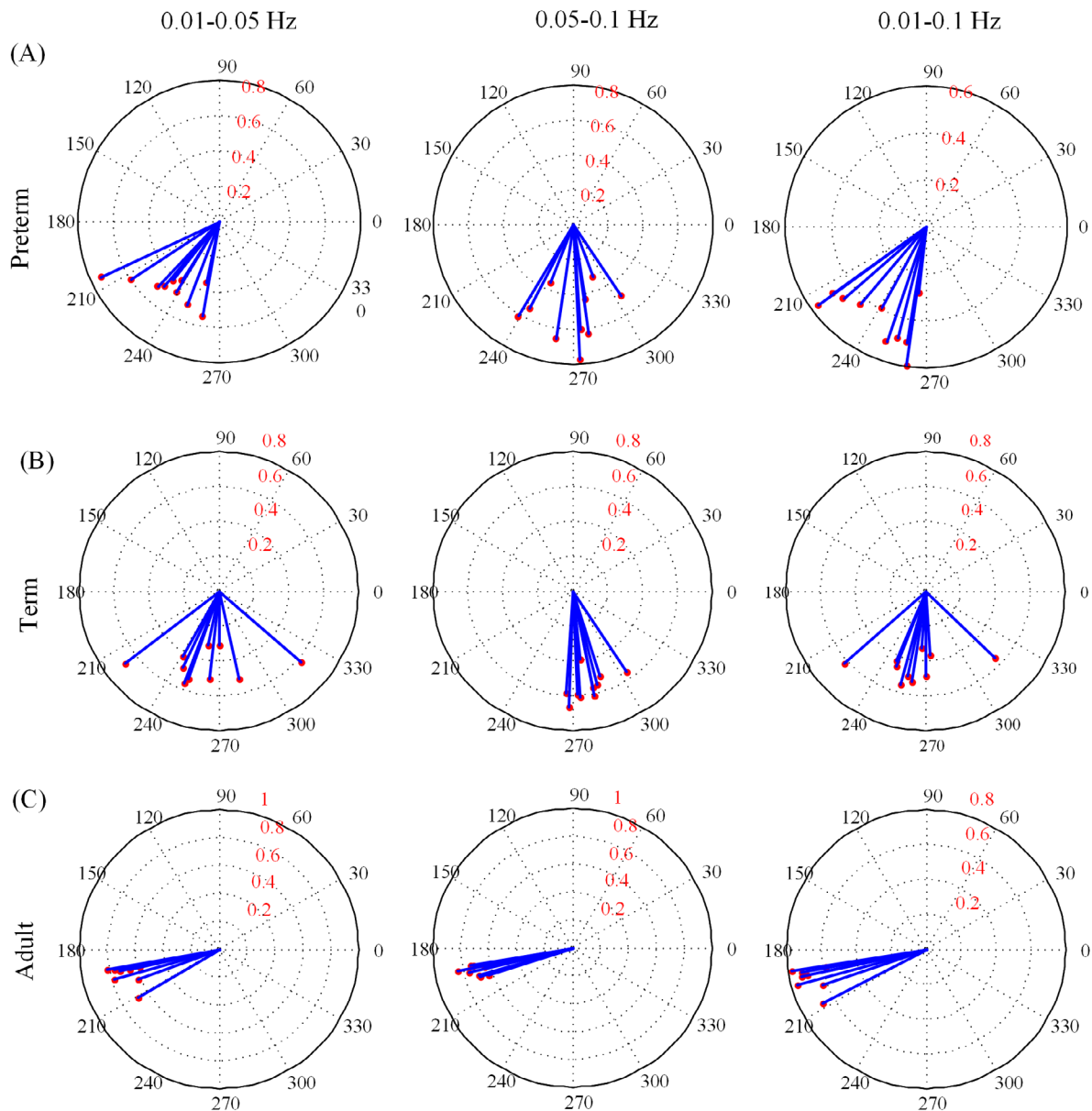


Figure 8. Vector representation of $hPod$ and $hPod_L$ (length of the vector) for preterm (A), term (B) and adults (C) in 0.01–0.05 Hz, 0.05–0.1 Hz, and 0.01–0.1 Hz, respectively.

different brain development states. The overlaps of these three types of measures (i.e. $hPod$, IPE, and APE) between the adults and neonates (i.e. both term and preterm) were smaller than those between the term and preterm infants. Compared to the phase difference measures, the coupling strength measures (i.e. $hPod_L$ and PCMI) were less precise in distinguishing the preterm and term (see figure 10) neonates except for PCMI in the 0.05–0.1 Hz frequency band. The significant p -values of all indices were shown in table 6. PCMI with epoch lengths of the 30 s, 60 s, and 90 s can distinguish preterm and term stages in the 0.05–0.1 Hz frequency band, which is better than the parallel measure of $hPod_L$ (see figures 10 and S6).

Furthermore, the index assessments' robustness in different states is important in assessing brain development, especially in neonates. We calculated the CV of all measurements within

all subjects in different frequency bands. The CV values were shown in tables 7–9. Because the CV value is vulnerable to the mean and SD, to compare the CV of IPE, APE, and $hPod$ consistently, we projected the $hPod$ indices into the range of 0–1 (Liang *et al* 2016b). All the CV values of IPE and APE were smaller than those of $hPod$ in all frequency bands and the PCMI values in the 0.05–0.1 Hz frequency band, while the 30 s epoch length had the lowest CVs among all the measurements (0.07, 0.08, and 0.09). These results illustrated that IPE, APE, and PCMI had a higher tolerance for noise than $hPod$ and $hPod_L$.

Spatial differences are also an important issue in brain development evaluation. We analyzed all the measurements in the prefrontal and left and right temporal areas of the infants. However, in this study, the fNIRS data were collected only

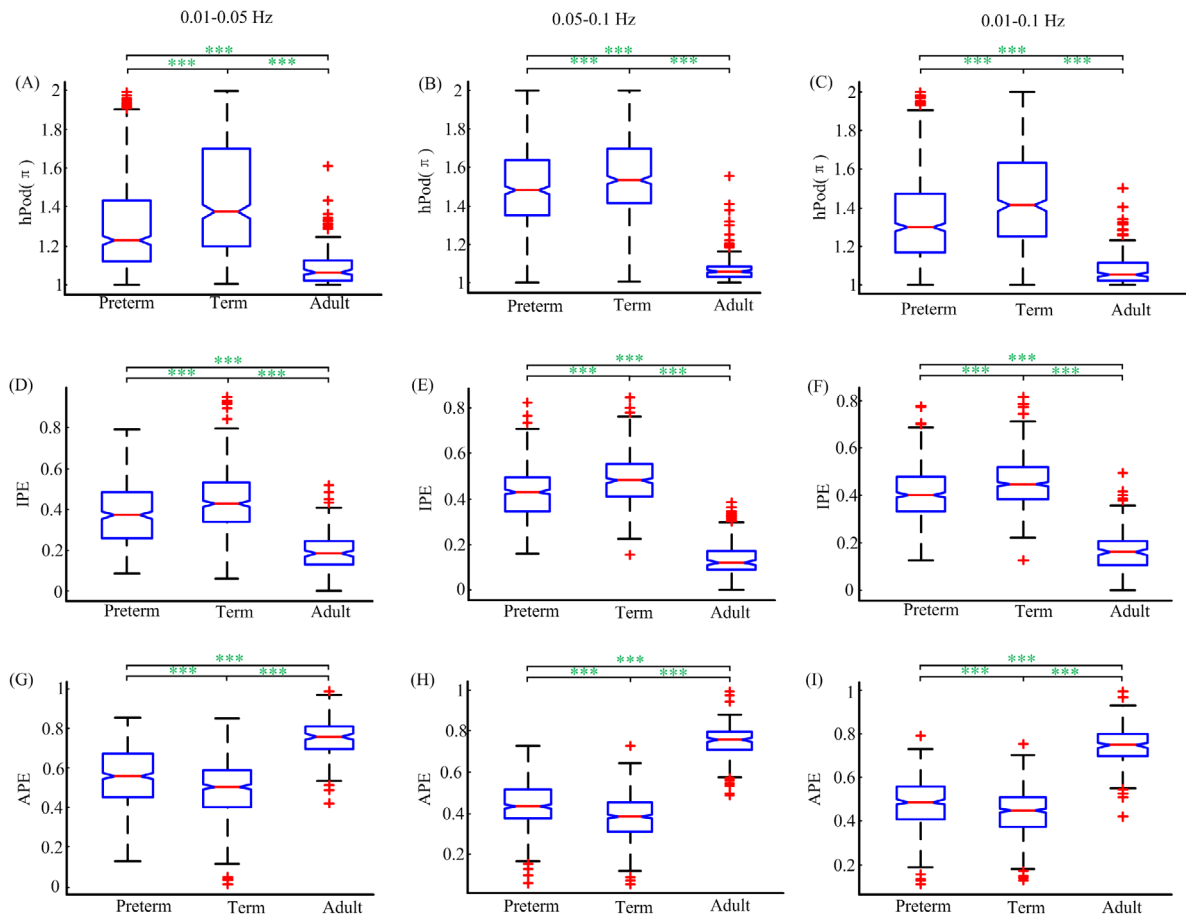


Figure 9. The statistics of the phase relationship measures indices. (A)–(C) The box plots of the hPod indices for preterm, term, and adults in 0.01–0.05 Hz, 0.05–0.1 Hz and 0.01–0.1 Hz, respectively. (D)–(F) The box plots of IPE indices for preterm, term and adults in the similar frequency bands with (A)–(C). (G)–(I) The box plots of IPE indices for preterm, term, and adult in the similar frequency bands with (A)–(C). The symbol of ‘***’ in each legend means that the p -value $p < 0.001/46 = 0.00002$.

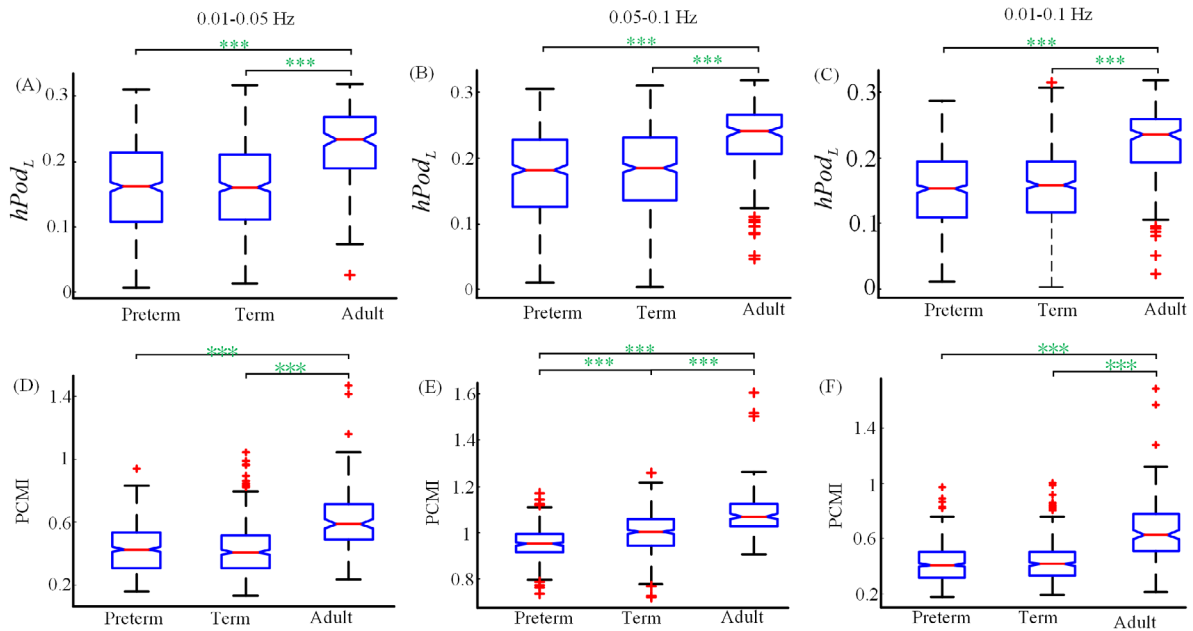


Figure 10. The statistics of the coupling strength measurements indices. (A)–(C) The box plots of $hPod_L$ indices for preterm, term, and adults in 0.01–0.05 Hz, 0.05–0.1 Hz and 0.01–0.1 Hz, respectively. (D)–(F) The box plots of PCMI indices for preterm, term, and adults in the similar frequency bands with (A)–(C). The symbol of ‘***’ in each legend means that the p -value $p < 0.001/46 = 0.00002$.

Table 3. The statistics of different measurements with preterm, term, and adults in 0.01–0.05 Hz.

	Preterm	Term	Adults
	Median (min-max)	Median (min-max)	Median (min-max)
hPod	1.23 (1.00–1.99)	1.37 (1.00–1.99)	1.06 (1.00–1.61)
IPE	0.37 (0.09–0.79)	0.43 (0.06–0.95)	0.18 (0–0.52)
APE	0.56 (0.13–0.85)	0.51 (0.01–0.85)	0.75 (0.42–0.98)
$hPod_L$	0.51 (0.02–0.97)	0.50 (0.04–0.99)	0.73 (0.08–0.99)
PCMI	0.43 (0.16–0.94)	0.41 (0.13–1.04)	0.59 (0.23–1.46)

hPod = hemoglobin phase of oxygenation and deoxygenation.

IPE = in-pattern exponent.

APE = anti-pattern exponent.

$hPod_L$ = phase-locking index of hPod.

PCMI = permutation cross mutual information with $m = 3, \tau = 11$.

Table 4. The statistics of different measurements with preterm, term, and adults in 0.05–0.1 Hz.

	Preterm	Term	Adults
	Median (min-max)	Median (min-max)	Median (min-max)
hPod	1.48 (1.00–1.99)	1.53 (1.00–1.99)	1.05 (1.00–1.56)
IPE	0.43 (0.16–0.82)	0.48 (0.16–0.85)	0.12 (0–0.39)
APE	0.43 (0.06–0.72)	0.38 (0.05–0.73)	0.75 (0.49–0.99)
$hPod_L$	0.57 (0.03–0.95)	0.58 (0.01–0.97)	0.75 (0.14–0.99)
PCMI	0.95 (0.74–1.17)	1.00 (0.74–1.26)	1.07 (0.91–1.60)

from the prefrontal area of adults. Hence, we can only compare the prefrontal area measurements of infants and adults. The arrangement of fNIRS channels and brain partition in infants are shown in figure S7, and a detailed analysis of all measurements was presented in supplementary appendix E. There were significant differences in the prefrontal area among preterm term neonates and adults based on the phase difference measurements (i.e. APE, IPE, and hPod) ($p < 0.00002$). However, these indices were not consistent with each other in distinguishing preterm and term infants in the left and right temporal regions. The coupling strength measurements ($hPod_L$ and PCMI) can also differentiate between infant and adult brains in the prefrontal area, although there was no significant difference between preterm and term. Only the PCMI in the 0.05–0.1 Hz frequency band more precisely distinguished between preterm and term infants in the left and right temporal areas (see figure S12).

5. Discussion and conclusions

Although brain development in neonates has been studied for a long time, and many fNIRS/fMRI algorithms have been proposed, no widely accepted theory has been established (Gu et al 2017, Watanabe et al 2017, Taga et al 2018). The fNIRS and fMRI literature indicated that the hemodynamic response curve changes with age (Issard and Gervain 2018) and the relative phase between the HbO and Hb can reflect complex interactions in neurovascular and metabolic development (Fantini 2002, Obrig and Villringer 2003, Boas et al 2008). There are

Table 5. The statistics of different measurements with preterm, term, and adults in 0.01–0.1 Hz.

	Preterm	Term	Adults
	Median (min-max)	Median (min-max)	Median (min-max)
hPod	1.29 (1.00–1.99)	1.41 (1.00–1.99)	1.05 (1.00–1.56)
IPE	0.40 (0.13–0.78)	0.45 (0.12–0.81)	0.16 (0–0.49)
APE	0.49 (0.11–0.79)	0.45 (0.13–0.75)	0.75 (0.42–0.99)
$hPod_L$	0.48 (0.03–0.90)	0.50 (0.01–0.99)	0.73 (0.07–0.99)
PCMI	0.41 (0.17–0.97)	0.42 (0.19–1.00)	0.63 (0.21–1.68)

Table 6. The p -values of different measurements with preterm, term, and adults in 0.01–0.1 Hz, 0.05–0.1 Hz and 0.01–0.1 Hz.

	Preterm-term	Preterm-adults	Term-adults
hPod	***/**/***	***/**/***	***/**/***
IPE	***/**/***	***/**/***	***/**/***
APE	***/**/***	***/**/***	***/**/***
$hPod_L$	o/o/o	***/**/***	***/**/***
PCMI	o/ ***/ o	***/**/***	***/**/***

The symbols, ‘o’, ‘*’, ‘**’ and ‘***’ indicate the p -values $p > 0.05/46 = 0.001, p < 0.05/46 = 0.001, p < 0.01/46 = 0.0002$ and $p < 0.001/46 = 0.00002$, respectively. The combination symbols ‘***/**/***’ represent the p -values in 0.01–0.05 Hz, 0.05–0.1 Hz and 0.01–0.1 Hz, respectively. The Kruskal–Wallis test and Multiple comparison were applied.

Table 7. The CV indices of different measurements with preterm, term, and adults in 0.01–0.05 Hz.

	Preterm	Term	Adults
hPod	0.80	0.65	1.08
IPE	0.36	0.32	0.48
APE	0.24	0.29	0.12
$hPod_L$	0.44	0.41	0.25
PCMI	0.34	0.37	0.30

many different ways to measure age-dependent phase changes in neonates, especially the phase synchronization methodology based on the Hilbert transform (Taga et al 2000, Imai et al 2014). The goal of these studies was to investigate more effective and robust methodologies to evaluate brain development. Motivated by this goal, in this study, we attempted to evaluate several novel methods (i.e. IPE, APE, and PCMI) based on symbolic dynamics and information theory in assessing brain development. IPE’s, APE’s and PCMI’s performance were compared to those of hPod and $hPod_L$ indices in both simulated and real fNIRS data. Results indicated that IPE and APE can effectively demarcate preterm and term infants and adults, and had smaller CV indices in all three different frequency bands than hPod. Furthermore, PCMI was superior in distinguishing neonates and adults than $hPod_L$, especially in the 0.05–0.1 Hz frequency band. A comparison and statistical analysis based on coupled nonlinear models also showed that symbolic dynamics-based measurements made more accurate predictions in tracking coupling strength.

One possible explanation is that IPE, APE, and PCMI are calculated based on the time series’ order patterns, which

Table 8. The CV indices of different measurements with preterm, term, and adults in 0.05–0.1 Hz.

	Preterm	Term	Adults
hPod	0.43	0.37	1.04
IPE	0.26	0.21	0.57
APE	0.25	0.26	0.12
$hPod_L$	0.40	0.36	0.24
PCMI	0.07	0.08	0.09

Table 9. The CV indices of different measurements with preterm, term, and adults in 0.01–0.1 Hz.

	Preterm	Term	Adults
hPod	0.67	0.57	1.04
IPE	0.25	0.22	0.51
APE	0.22	0.23	0.11
$hPod_L$	0.40	0.37	0.25
PCMI	0.32	0.32	0.34

combines mutual information, symbolic dynamics, and non-linear system theories. hPod and $hPod_L$ are based on the FFT and Hilbert transform, which implicitly assumes that the physiological records are sums of periodical stationary signals. However, IPE, APE, and PCMI are based on the patterns' sequential information, so this symbolic transform focuses on the temporal relationship between neighboring points instead of the oscillation magnitude (Bandt and Pompe 2002). Hence, the phase relationship (APE and IPE) and coupling strength (PCMI) obtained from HbO and Hb signals at different stages will be presented in symbolic synchronization and mutual information. Moreover, compared to FFT and Hilbert transform based algorithms (hPod and $hPod_L$), symbolic dynamics and mutual information methodologies are nonparametric and required limited computing power (Bahraminasab *et al* 2008). Furthermore, it does not need any underlying assumption that the time series or oscillations are stationary or sinusoidal (Talebinejad *et al* 2011). More importantly, mutual information and symbolic transform analysis offer a unique perspective to estimate complex hemodynamic and neurovascular changes during brain development (e.g. the coupling strength of the HbO and Hb become stronger as the cerebral vascular system and neurovascular and metabolic functions develop). Lastly, as described in our previous studies, the symbolic dynamic and mutual information measures were insensitive to the time series' amplitude, making them more tolerant to noise (Abásolo *et al* 2006, Ferenets *et al* 2006, Liang *et al* 2015). Therefore, all these merits indicated the great potential of IPE, APE, and PCMI to be outstanding nonlinear measurements in evaluating brain development changes using fNIRS signals.

Although fNIRS can not measure neuronal activation directly, it can measure HbO and Hb concentration changes, which can be caused by changes in blood flow/volume, or neuronal activation through the neurovascular coupling. In this study, we systematically measured phase changes between Hb and HbO among infants during sleep (no stimulation). We will interpret the results from the perspective of

the cerebrovascular development. From a previous study, it is known that brain development will cause the following vascular changes. (1) increased blood volume due to growing capillary density; (2) increased capillary and venous blood flow; and (3) increased mean arterial pressure (limited by cerebral auto-regulation (Greisen 2005)). In addition to these vascular changes, Franceschini *et al* found that there were regionally specific increases in oxygen consumption in healthy infants during their first year (Franceschini *et al* 2007). Interestingly, based on the model (Fantini 2014), increased cerebral blood volume has an in-phase contribution to the phase difference of HbO and Hb, whereas increases in the partial pressure of oxygen, oxygen utilization rate, and speed of blood flow have an anti-phase effect (Watanabe *et al* 2017). In this study, we found that infants with a higher post-natal age (preterm infants (mean: 23.7 d, range: 17–35 d) have a higher anti-phase trend (compared to term infants with mean: 4.2 d, range: 3–6 d). Thus, our study implies that growth of the partial pressure of oxygen, oxygen utilization rate and speed of blood flow is the dominant effect in infants' development, which outweigh that of cerebral blood volume increase. This growth likely stabilizes after six months, resulting in a constant phase difference between HbO and Hb that are maintained into adulthood (Watanabe *et al* 2017).

We reached the conclusions that the hPod, IPE, and APE indices have the similar group mean values in 0.01–0.05 Hz and 0.05–0.1 Hz frequency bands, which are consistent with a previous study (Watanabe *et al* 2017). From the perspective of coupling measurement, the coupling measure of PCMI indices shows a significant difference between term and preterm infants only in the 0.05–0.1 Hz frequency band (see figures 10 and S6) ($p < 0.0002$). However, we do not know what underlying physiological changes made the 0.05–0.1 Hz signal more sensitive to brain development for PCMI. Frequency dependence is an open question in fNIRS and fMRI resting-state studies. We believe that multimodal studies using EEG and fNIRS/fMRI, or animal studies could be exploited to deepen our understanding of this issue.

In this study, the most important finding is the identification of parameters that can distinguish term and preterm infants. For these two groups of infants, channel locations, measurement devices, and recording durations were exactly the same. The fNIRS measurements of adults only covered the prefrontal area, which was not ideal. However, we do not think it would change the results for the following reasons. First, many studies of healthy adults have observed the same anti-phase relationship of HbO and Hb oscillations in many regions of the brain in both resting and task experiments (Issard and Gervain 2017, Lloyd-Fox *et al* 2017, Watanabe *et al* 2017). The measurements we performed should only be served as an example. Second, in this study, we found that the prefrontal region gave the most robust results for many parameters (e.g. IPE, APE, and hPod). This region was shared by infants and adults. Third, although different measurement devices were used for infants and adults, all the indices we analyzed were based on the phase or symbolic pattern of the signal, which is less sensitive to device selection. Finally, in both infants and

adults, the measurement times extended beyond 2 min, which has been proven sufficient to obtain a robust index.

However, there are some limitations that should be addressed. First, in this study, the number of datasets is relatively small and the preterm data set only contains early preterm neonates. In future studies, more subjects from a wider age range should be recruited. Second, the adults' experimental conditions were different from those of the infants, which may make direct comparisons difficult. More consistent experimental conditions will be sought in future studies.

In conclusion, the symbolic dynamic-based measures, IPE, APE, and PCMI, can measure brain development changes based on fNIRS signals. PCMI reflects the coupling strength of hemodynamic signals and, to some extent, reveals the underlying mechanisms of brain development. The potential of IPE, APE, and PCMI in estimating brain development has been demonstrated in this study. Furthermore, our new methods (IPE, APE, and PCMI) can be applied to fMRI data. However, instead of measuring HbO and Hb phase differences within one channel, these parameters can be used to assess coupling strength or phase differences between channels (voxels/regions of interest). We believe it will approach interesting brain interactions from a new perspective.

Acknowledgments

This research was supported by the National Natural Science Foundation of China (61673333, 61304247), Natural Science Fund for Excellent Young Scholars of Hebei Province of China (F2018203281), Grant-in-Aid for Scientific Research (KAKENHI) (A) (24118508) (YM) and National Institutes of Health (USA), Grants K25 DA031769 (YT). Dr Zhenhu Liang received support from the China Scholarship Council.

Disclosure

The authors declare no conflict of interest.

ORCID iDs

Zhenhu Liang  <https://orcid.org/0000-0002-2467-9877>

References

- Abásolo D, Hornero R, Gómez C, García M and López M 2006 Analysis of EEG background activity in Alzheimer's disease patients with Lempel–Ziv complexity and central tendency measure *Med. Eng. Phys.* **28** 315–22
- Amigo J M, Keller K and Unakafova V A 2015 Ordinal symbolic analysis and its application to biomedical recordings *Phil. Trans. R. Soc. A* **373** 20140091
- Andrzejak R G, Kraskov A, Stogbauer H, Mormann F and Kreuz T 2003 Bivariate surrogate techniques: necessity, strengths, and caveats *Phys. Rev. E* **68** 066202
- Arimitsu T, Minagawa Y, Yagihashi T, Uchida M O, Matsuzaki A, Ikeda K and Takahashi T 2018 The cerebral hemodynamic response to phonetic changes of speech in preterm and term infants: The impact of postmenstrual age *NeuroImage Clin.* **19** 599–606
- Bahraminasab A, Ghasemi F, Stefanovska A, McClintock P V and Kantz H 2008 Direction of coupling from phases of interacting oscillators: a permutation information approach *Phys. Rev. Lett.* **100** 084101
- Bandt C and Pompe B 2002 Permutation entropy: a natural complexity measure for time series *Phys. Rev. Lett.* **88** 174102
- Benavides-Varela S, Siugzdaite R, Gomez D M, Macagno F, Cattarossi L and Mehler J 2017 Brain regions and functional interactions supporting early word recognition in the face of input variability *Proc. Natl Acad. Sci. USA* **114** 7588–93
- Berens P 2009 CircStat: a MATLAB toolbox for circular statistics *J. Stat. Softw.* **31** 1–21
- Bießmann F, Plis S, Meinecke F C, Eichele T and Müller K-R 2011 Analysis of multimodal neuroimaging data *IEEE Rev. Biomed. Eng.* **4** 26–58
- Boas D A, Jones S R, Devor A, Huppert T J and Dale A M 2008 A vascular anatomical network model of the spatio-temporal response to brain activation *NeuroImage* **40** 1116–29
- Chiarelli A M, Maclin E L, Fabiani M and Gratton G 2015 A kurtosis-based wavelet algorithm for motion artifact correction of fNIRS data *NeuroImage* **112** 128–37
- Cohen L, Loughlin P and Vakman D 1999 On an ambiguity in the definition of the amplitude and phase of a signal *Signal Process.* **79** 301–7
- Cole S R and Voytek B 2017 Brain oscillations and the importance of waveform shape *Trends Cogn. Sci.* **21** 137–49
- Dalmis M U and Akin A 2015 Similarity analysis of functional connectivity with functional near-infrared spectroscopy *J. Biomed. Opt.* **20** 86012
- Daw C S, Finney C E A and Tracy E R 2003 A review of symbolic analysis of experimental data *Rev. Sci. Instrum.* **74** 915–30
- Edwards R, Siegelmann H T, Aziza K and Glass L 2001 Symbolic dynamics and computation in model gene networks *Chaos* **11** 160–9
- Fantini S 2002 A haemodynamic model for the physiological interpretation of *in vivo* measurements of the concentration and oxygen saturation of haemoglobin *Phys. Med. Biol.* **47** N249
- Fantini S 2014 Dynamic model for the tissue concentration and oxygen saturation of hemoglobin in relation to blood volume, flow velocity, and oxygen consumption: implications for functional neuroimaging and coherent hemodynamics spectroscopy (CHS) *NeuroImage* **85** 202–21
- Ferenets R, Lipping T, Anier A, Jantti V, Melto S and Hovilehto S 2006 Comparison of entropy and complexity measures for the assessment of depth of sedation *IEEE Trans. Biomed. Eng.* **53** 1067–77
- Ferlazzo E et al 2014 Permutation entropy of scalp EEG: a tool to investigate epilepsies: suggestions from absence epilepsies *Clin. Neurophysiol.* **125** 13–20
- Franceschini M A, Thaker S, Themelis G, Krishnamoorthy K K, Bortfeld H, Diamond S G, Boas D A, Arvin K and Grant P E 2007 Assessment of infant brain development with frequency-domain near-infrared spectroscopy *Pediatr. Res.* **61** 546–51
- Greisen G 2005 Autoregulation of cerebral blood flow in newborn babies *Early Hum. Dev.* **81** 423–8
- Gu Y, Miao S, Han J, Zeng K, Ouyang G, Yang J and Li X 2017 Complexity analysis of fNIRS signals in ADHD children during working memory task *Sci. Rep.* **7** 829
- Homae F, Watanabe H, Otobe T, Nakano T, Go T, Konishi Y and Taga G 2010 Development of global cortical networks in early infancy *J. Neurosci.* **30** 4877–82
- Imai M, Watanabe H, Yasui K, Kimura Y, Shitara Y, Tsuchida S, Takahashi N and Taga G 2014 Functional connectivity of the cortex of term and preterm infants and infants with Down's syndrome *NeuroImage* **85** 272–8

- Issard C and Gervain J 2017 Adult-like processing of time-compressed speech by newborns: a NIRS study *Dev. Cogn. Neurosci.* **25** 176–84
- Issard C and Gervain J 2018 Variability of the hemodynamic response in infants: Influence of experimental design and stimulus complexity *Dev. Cogn. Neurosci.* in press (<https://doi.org/10.1016/j.dcn.2018.01.009>)
- Khoa T Q, Thang H M and Nakagawa M 2008 Testing for nonlinearity in functional near-infrared spectroscopy of brain activities by surrogate data methods *J. Physiol. Sci.* **58** 47–52
- Kreuz T, Mormann F, Andrzejak R G, Kraskov A, Lehnertz K and Grassberger P 2007 Measuring synchronization in coupled model systems: a comparison of different approaches *Physica D* **225** 29–42
- Lachaux J P, Rodriguez E, Martinerie J and Varela F J 1999 Measuring phase synchrony in brain signals *Hum. Brain Mapp.* **8** 194–208
- Li D, Li X, Cui D and Li Z 2011 Phase synchronization with harmonic wavelet transform with application to neuronal populations *Neurocomputing* **74** 3389–403
- Li X and Ouyang G 2010 Estimating coupling direction between neuronal populations with permutation conditional mutual information *NeuroImage* **52** 497–507
- Li X, Li D, Liang Z, Voss L J and Sleigh J W 2008 Analysis of depth of anesthesia with Hilbert–Huang spectral entropy *Clin. Neurophysiol.* **119** 2465–75
- Liang Z, Bai Y, Ren Y and Li X 2016a Synchronization measures in EEG signals *Signal Processing in Neuroscience* ed X Li (Berlin: Springer) pp 167–202
- Liang Z, Liang S, Wang Y, Ouyang G and Li X 2015 Tracking the coupling of two electroencephalogram series in the isoflurane and remifentanyl anesthesia *Clin. Neurophysiol.* **126** 412–22
- Liang Z, Ren Y, Yan J, Li D, Voss L J, Sleigh J W and Li X 2016b A comparison of different synchronization measures in electroencephalogram during propofol anesthesia *J. Clin. Monit. Comput.* **30** 451–66
- Lloyd-Fox S et al 2017 Cortical specialisation to social stimuli from the first days to the second year of life: a rural Gambian cohort *Dev. Cogn. Neurosci.* **25** 92–104
- Martini M, Kranz T A, Wagner T and Lehnertz K 2011 Inferring directional interactions from transient signals with symbolic transfer entropy *Phys. Rev. E* **83** 186–96
- Montani F, Rosso O A, Matias F S, Bressler S L and Mirasso C R 2015 A symbolic information approach to determine anticipated and delayed synchronization in neuronal circuit models *Phil. Trans. R. Soc. A* **373** 20150110
- Mwaniki M K, Atieno M, Lawn J E and Newton C R 2012 Long-term neurodevelopmental outcomes after intrauterine and neonatal insults: a systematic review *Lancet* **379** 445–52
- Norman M G and O’Kusky J R 1986 The growth and development of microvasculature in human cerebral cortex *J. Neuropathol. Exp. Neurol.* **45** 222–32
- Obrig H and Villringer A 2003 Beyond the visible—imaging the human brain with light *J. Cerebr. Blood Flow Metab.* **23** 1–18
- Oliveira P M and Barroso V 1999 Instantaneous frequency of multicomponent signals *IEEE Signal Process. Lett.* **6** 81–3
- Paluš M 1996 Coarse-grained entropy rates for characterization of complex time series *Physica D* **93** 64–77
- Palus M and Stefanovska A 2003 Direction of coupling from phases of interacting oscillators: an information-theoretic approach *Phys. Rev. E* **67** 055201
- Palus M and Vejmelka M 2007 Directionality of coupling from bivariate time series: how to avoid false causalities and missed connections *Phys. Rev. E* **75** 056211
- Perpetuini D, Bucco R, Zito M and Merla A 2018 Study of memory deficit in Alzheimer’s disease by means of complexity analysis of fNIRS signal *Neurophotonics* **5** 011010
- Pinti P, Cardone D and Merla A 2015 Simultaneous fNIRS and thermal infrared imaging during cognitive task reveal autonomic correlates of prefrontal cortex activity *Sci. Rep.* **5** 17471
- Pockett S, Bold G E and Freeman W J 2009 EEG synchrony during a perceptual-cognitive task: widespread phase synchrony at all frequencies *Clin. Neurophysiol.* **120** 695–708
- Pouliot P, Tremblay J, Robert M, Vannasing P, Lepore F, Lassonde M, Sawan M, Nguyen D K and Lesage F 2012 Nonlinear hemodynamic responses in human epilepsy: a multimodal analysis with fNIRS-EEG and fMRI-EEG *J. Neurosci. Methods* **204** 326–40
- Quaresima V, Bisconti S and Ferrari M 2012 A brief review on the use of functional near-infrared spectroscopy (fNIRS) for language imaging studies in human newborns and adults *Brain Lang.* **121** 79–89
- Ray A 2004 Symbolic dynamic analysis of complex systems for anomaly detection *Signal Process.* **84** 1115–30
- Roche-Labarbe N, Carp S A, Surova A, Patel M, Boas D A, Grant P E and Franceschini M A 2010 Noninvasive optical measures of CBV, StO(2), CBF index, and rCMRO(2) in human premature neonates’ brains in the first six weeks of life *Hum. Brain Mapp.* **31** 341–52
- Sassaroli A, Kainerstorfer J M and Fantini S 2016 Nonlinear extension of a hemodynamic linear model for coherent hemodynamics spectroscopy *J. Theor. Biol.* **389** 132–45
- Schiff S J, So P, Chang T, Burke R E and Sauer T 1996 Detecting dynamical interdependence and generalized synchrony through mutual prediction in a neural ensemble *Phys. Rev. E* **54** 6708
- Streimish I G, Ehrenkranz R A, Allred E N, O’Shea T M, Kuban K C, Paneth N and Leviton A 2012 Birth weight- and fetal weight-growth restriction: impact on neurodevelopment *Early Hum. Dev.* **88** 765–71
- Taga G, Konishi Y, Maki A, Tachibana T, Fujiwara M and Koizumi H 2000 Spontaneous oscillation of oxy- and deoxy-hemoglobin changes with a phase difference throughout the occipital cortex of newborn infants observed using non-invasive optical topography *Neurosci. Lett.* **282** 101–4
- Taga G, Watanabe H and Homae F 2018 Spatial variation in the hemoglobin phase of oxygenation and deoxygenation in the developing cortex of infants *Neurophotonics* **5** 011017
- Talebinejad M, Chan A D and Miri A 2011 A Lempel–Ziv complexity measure for muscle fatigue estimation *J. Electromyogr. Kinesiol.* **21** 236–41
- Tan Q, Zhang M, Wang Y, Wang B, Xin Q and Li Z 2016 Age-related alterations in phase synchronization of oxyhemoglobin concentration changes in prefrontal tissues as measured by near-infrared spectroscopy signals *Microvasc. Res.* **103** 19–25
- Thomason M E et al 2017 Weak functional connectivity in the human fetal brain prior to preterm birth *Sci. Rep.* **7** 39286
- Volpe J J 2009 Brain injury in premature infants: a complex amalgam of destructive and developmental disturbances *Lancet Neurol.* **8** 110–24
- Wang K, Steyn-Ross M L, Steyn-Ross D A, Wilson M T and Sleigh J W 2014 EEG slow-wave coherence changes in propofol-induced general anesthesia: experiment and theory *Frontiers Syst. Neurosci.* **8** 215
- Watanabe H, Shitara Y, Aoki Y, Inoue T, Tsuchida S, Takahashi N and Taga G 2017 Hemoglobin phase of oxygenation and deoxygenation in early brain development measured using fNIRS *Proc. Natl Acad. Sci. USA* **114** E1737–44
- Yin X, Xu B, Jiang C, Fu Y, Wang Z, Li H and Shi G 2015 Classification of hemodynamic responses associated with force and speed imagery for a brain-computer interface *J. Med. Syst.* **39** 53
- Zunino L, Olivares F and Rosso O A 2015 Permutation min-entropy: an improved quantifier for unveiling subtle temporal correlations *Eur. Phys. Lett.* **109** 10005